Macromolecules

pubs.acs.org/Macromolecules Article

Stretching and Bending Moduli of Bilayer Films Inferred from Wrinkle Patterns

Jooyoung Chang, Narayanan Menon, and Thomas P. Russell*

Cite This: *Macromolecules* 2024, 57, 10091−10097 Read Online

ACCESS | Metrics & More | Article Recommendations

ABSTRACT: Wrinkling patterns were used to investigate the mechanical properties of thin poly(styrene) (PS)/poly(methyl methacrylate) (PMMA) and PS/gold (Au) bilayer films. Films were floated on water with a water drop on the surface to induce wrinkling. The thicknesses and thickness ratios of the films were varied over a broad range. The PS/PMMA bilayer was chosen to provide a contrast in wetting properties, with equilibrium contact angles of θ_{PMMA} = 68° and θ_{PS} = 88° with water. The PS/Au bilayer was chosen to provide a large contrast in Young's moduli, E_{Au} = 72 GPa and E_{PS} = 3.4 GPa. The stretching (Y) and bending (B) moduli of the bilayer films were obtained from measurements of the length and number of wrinkles in the wrinkle patterns. The experimentally derived values of Y and B were in reasonable agreement with the values computed from the bulk Young's moduli and the thicknesses of the two components in the bilayer. The values of Y and B did not depend on which face of the film was exposed to the water droplet or bath when the capillary stresses were considered. Thus, finite size effects from the film thicknesses were unimportant over the range of thicknesses studied, and no relative displacement of the films was found, with the films remaining well-bonded even with deformation associated with wrinkling.

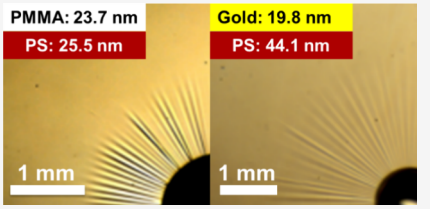

INTRODUCTION

Due to the rapid growth in demand for small-scale devices, multilayer nanoscale structures have been used extensively as a key element in the design and performance of devices. Therefore, accurate determination of the mechanical properties of the multilayer films is necessary. Elucidation of the strength and reliability of these devices with current nanotechnologies has been extremely challenging. This is of importance for the design, processing, testing, and packaging of flexible electronic devices, semiconductors, photoresists, solar cells, and coatings. Different organic, polymeric, polymer−metal, polymer-inorganic, or inorganic-metal hybrid materials have been used in these devices to simultaneously enhance performance and rigidity; yet, understanding which properties, e.g. surface energies or Young's moduli, dictate the mechanical behavior is limited. Numerous experiments using a wide range of techniques have been reported to study the mechanical properties of films nanometers in thickness.[1−36] Most have focused on the variation in glass transition temperature (T_g) or Young's modulus as a function of film thickness.[5,14,17,20,21,28,36−50] Experimental results on T_g are varied, and this is still a topic of debate.[2,4−6,14,17−19,40,45,51] Experimental results on Young's moduli of single-layer films have suggested a decrease in the elastic modulus when the thickness of the film was below a critical value, dependent, although, on the experimental technique used.[21,28,48−50,52,53] To remove the residual shear stresses from films on solid substrates, studies have also been performed on liquid surfaces to measure compliance, T_g, elastic modulus, strain, viscosity, and dewetting.[2,33,45,54−57] A recent review article discusses many mechanical and rheological methods to determine the material properties of glassy polymers under confinement.[58] Mechanical properties have been determined by the wrinkling of thin films floating on liquid surfaces using out-of-plane deformation. Consequently, tangential shear stresses in the film from the substrate are removed, and the deformation is easily measured by noncontact probes. The reversibility of the deformation in the linear elasticity regime is simply confirmed by removing the external perturbation.

Here, we investigated the stretching (Y) and bending (B) moduli of unconstrained, stress-relaxed PS/PMMA and PS/Au bilayers by using capillary wrinkling. Bilayer films were floated onto water, and a drop of water in the center of the film induced a wrinkle pattern. Y and B were determined from the characteristics of the wrinkling pattern using a far-from-threshold (FT) analysis of the wrinkling instability.[59] From these two pairs of materials, we investigated the influence of surface energies and bulk moduli on the mechanical properties of the bilayer. The total thicknesses of the bilayer films varied from 34 to 884 nm for PS/PMMA films and from 49.6 to 495 nm for PS/Au films. The ratio of the thickness of the two layers in

Received: July 6, 2024
Revised: September 19, 2024
Accepted: October 8, 2024
Published: October 23, 2024

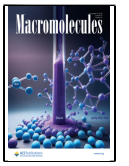

https://doi.org/10.1021/acs.macromol.4c01540
Macromolecules 2024, 57, 10091−10097

the film was also varied over a large range. For both types of films, capillary forces were generated with the PS or PMMA layer, in one case, or the PS or Au layer, in the other case, in contact with the underlying liquid. Y and B of the films, determined from the length and number of wrinkles, compare well with those calculated from a weighted average using the bulk Young's moduli of the individual layers. This is meaningful since the results show that the appropriately thickness-weighted averages of Y and B in eqs 2 and 4 can estimate the mechanical properties of bilayer thin films. In addition, this also shows that this metrology can be a useful approach to understanding the mechanical behaviors of bilayer thin films, broadening the scope of fin-thin film metrology.

EXPERIMENTAL METHODS

PMMA (M_w = 99.6 kg/mol, with a syndio:hetero:isotactic content of 55:37:8) and poly(acrylic acid) (PAA) solution ($M_w \sim$ 100 kg/mol, 35 wt % in water) were purchased from Sigma-Aldrich. PS (M_w = 97 kg/mol, M_w/M_n = 1.06) was purchased from the Polymer Source. Gold pellets (1/4″ diameter ×1/4″ length, purity 99.999%) were purchased from Kurt J. Lesker. PS and PMMA were used without further purification. PS was dissolved in either toluene (anhydrous, 99.8%, Sigma-Aldrich) or 1-chloropentane (99%, Sigma-Aldrich) to produce concentrations varying from 0.8 to 7 wt %. PMMA was dissolved in anisole (anhydrous, 99.8%, Sigma-Aldrich) to produce 0.8 to 6 wt %. solutions of PMMA.[60]

To construct PS (top)/PMMA (bottom) bilayers, a sequential spin-coating onto 3 cm × 3 cm Si substrates with a 250 nm oxide layer was used since 1-chloropentane is a good solvent for PS and a nonsolvent for PMMA. The Si substrates were cleaned using a carbon dioxide snow jet and UV-Ozone (JElight, Model No.342) for 10 min before use. Solutions were filtered through 0.45 mm Whatman PTFE filters to remove impurities and then directly applied to the substrate. Different spin-coating speeds (1200 to 4000 rpm) were used to vary the layer thicknesses (47.5 to 810.4 nm). The spin-coated films were dried under ambient conditions for 2 days to remove residual solvent and stress. A water-transfer method was also used to remove the PMMA/PS bilayer films from the substrate. PS and PMMA films were spin-coated on separate, precleaned silica wafers. The spin-coated and dried PMMA films were floated onto the surface of water and retrieved on a substrate coated with the dried PS film. The bilayer films were dried under ambient conditions to remove residual water.[61] Various concentrations of solution (0.6 wt % ∼ 5.5 wt %) and a wide range of spinning speeds (1200 rpm ∼ 4000 rpm) were used to vary the total thicknesses of the PMMA/PS and PS/PMMA (33.6−884.3 nm) bilayer films.

PS/Au and Au/PS bilayer films were constructed by using different methods. The Au (top)/PS (bottom) bilayer films were obtained by sequential spin-coating and thermal evaporation. Solutions with different PS concentrations in toluene (1.8−5.5 wt %) were filtered and spin-coated onto precleaned substrates at varying spinning speeds (1000 to 6000 rpm) to control the thicknesses of the PS layer. The spin-coated PS films were then dried under ambient conditions for 2 days to remove residual solvent and stress. Au films were thermally evaporated onto spin-coated PS films. Under the evaporation conditions used, Au at the surface of PS film was consistently measured at 60 °C, avoiding annealing the films above the T_g of PS film. To prepare a bilayer with PS (top)/Au (bottom), a 35 wt % solution of PAA in water was diluted to 5 wt % with deionized water. This was spin-coated onto the 3 × 3 cm^2 substrate to produce a 100 nm thick PAA film, then annealed at 140 °C for 1.5 min to remove residual water. A 20 ± 3.9 nm layer of Au was thermally evaporated onto the PAA film to produce the bilayer. The water-soluble PAA layer was absent, and the poor adhesion between the silica substrate and thermally evaporated Au film led to multiple fractures of the Au film when floated onto a water surface. PS solutions with different concentrations (1−5.5 wt %) were dissolved in toluene. The PS solutions were spin-coated onto the 20 ± 3.9 nm thick Au films to produce PS/Au bilayer films with thicknesses from 49.6 to 452.3 nm. The PS/Au bilayer films were dried for 2 days to remove residual stress and solvent.

Bilayer films were cut into 15 mm diameter disks by using a tungsten carbide scribe and floated onto the surface of water. A 0.2−0.3 μL water droplet was placed at the center of the floating bilayer film with a microsyringe (Hamilton, CAT#80383). The volume of the droplet was then increased in 0.2 μL increments until a maximum volume of ∼1 μL. Images of the resultant wrinkle pattern at each droplet size were taken with a digital single-lens reflex camera (Nikon D7100) mounted on a stereo microscope (Olympus SZ 40). The images were analyzed using ImageJ and MATLAB to determine the length and number of wrinkles. After measurement, the bilayer films were retrieved with a silicon substrate using a precleaned 250 nm thick SiO_2 layer and dried for 2−3 days to remove all the residual water for storage or future use. The film thicknesses of the dried bilayer films were determined by using a Filmetrics F20−UV spectral reflectance interferometer.

DATA ANALYSIS

Stretching (Y) and Bending (B) Moduli of Bilayer Films.

The mechanical moduli for bilayer films can be determined from those for single-layer films. For the stretching modulus, we have the expressions below:[61,62]

$$Y_{single} = Et \tag{1}$$

$$Y_{Bi} = E_1 t_1 + E_2 t_2 \tag{2}$$

where E is the Young's modulus, and t is the film thickness. Subscripts 1 and 2 indicate the top and bottom layers, respectively, of the floating bilayer. The physics behind the expression for the bilayer stretching modulus is relatively transparent, representing the two layers as springs that are in parallel. The in-plane stresses are different in the layers, but the displacement is continuous at the boundary between the layers if the two layers are in intimate contact. The bending moduli are determined from

$$B_{single} = \frac{Et^3}{12(1-\Lambda^2)} \tag{3}$$

$$B_{Bi} = \frac{E_1 t_1 E_2 t_2 \left(\frac{t_1+t_2}{2}\right)^2}{(1-\Lambda_2^2)E_1 t_1 + (1-\Lambda_1^2)E_2 t_2} + \frac{1}{12}\left[\frac{E_1 t_1^3}{1-\Lambda_1^2} + \frac{E_2 t_2^3}{1-\Lambda_2^2}\right] \tag{4}$$

where Λ is the Poisson ratio for the bulk material.[62−64] When a homogeneous film is uniaxially bent through a radius of curvature, then the outer surface of the film is under tension while the inner surface is under compression. In the interior of the film, there is an imaginary plane known as the neutral plane, which is unstressed. Integrating through the thickness of the film yields eq 3 for the bending rigidity of a uniform film. Similar considerations apply to bending a double layer; however, if there is a contrast in Young's modulus of the two layers, more of the strain resides in the softer material, and the neutral plane is shifted accordingly. This leads to a nontrivial weighting between bending rigidities of 1 and 2 in eq 4 for the bending rigidity of the composite bilayer. Note that bending in either direction carries the same value of B, and this is a considerable simplification, as a wrinkle pattern involves alternating the sign of the curvature from peak to valley and back to peak. These formulas assume that (i) there are no finite-thickness effects due to the R_g of the polymer and that the bulk value of Young's modulus can be used for the thin films, (ii) the films are well-bonded to one another,

https://doi.org/10.1021/acs.macromol.4c01540
Macromolecules 2024, 57, 10091−10097

with no relative displacement at the interface between the films, and (iii) the surface on which the capillary force is applied can be accounted for by using the appropriate wetting angles and surface energies. These assumptions were tested by comparing the predictions with experimentally determined values of Y and B.

The relevant bulk material properties obtained from the literature for our materials are $E_{PS} = 3.4$ GPa, $E_{PMMA} = 3.0$ GPa, $E_{Au} = 72$ GPa, $\Lambda_{PS\ or\ PMMA} = 0.34$, $\Lambda_{Au} = 0.42$. The thicknesses of the films were varied over a large range in our experiments.

Extracting Bending and Stretching Modulus from Wrinkling Patterns. Whenever there is a large enough compressive stress in a thin film, wrinkles form orthogonal to the compression direction. When a film is floating on the surface of water, it experiences a radial tension at its outer edge equal to the air−water tension (γ), and independent of the solid−liquid surface energy.[65] When a drop of liquid is placed on top of the floating film, there is an out-of-plane capillary force at the contact line, which leads to a boundary condition on the radial stress at the outer edge of the drop. These differential radial tensions on the outside and inside of the film can lead to a compressive tension $\sigma_{\theta\theta}$ in the azimuthal, or hoop, direction.[66] The azimuthal compression leads to the formation of wrinkles along the radial direction. When the scale of the capillary stresses (set by γ) is much larger than the characteristic buckling thresholds for the film, then it is no longer appropriate to use linear stability analysis to infer the size and wavenumber of the wrinkling pattern, but rather, a far-from-threshold (FT) analysis must be used. The FT predictions for the wrinkle length shown in eq 5 below are based on the assumption that, to the first order, the wrinkles come at no energetic cost ($B = 0$) and relax the compressive stress completely ($\sigma_{\theta\theta} = 0$).[59] Thus, the length of the wrinkles depends purely on Y in the limit of very thin films. At the next level of approximation, the finite cost of wrinkling due to a finite B is balanced against the energetic cost of deforming the subphase (gravitational potential energy of the water) and pulling against the radial tension. Thus, the number of wrinkles depends on B and on the overall radial state of tension.

Within this framework, the length of wrinkles, L, in the Far-from-Threshold (FT) regime was determined, as described elsewhere.[59,66,67] The hoop ($\sigma_{\theta\theta}$) and radial (σ_{rr}) stresses were calculated from the Lamé solution in a disc geometry under radial stress conditions, and from this, the length L of the wrinkles is predicted as a function of the applied capillary stress

$$L = \frac{\tau a}{2} \tag{5}$$

where τ is the confinement parameter given in eq 7 below and a is the radius of the water droplet on the film.

As previously reported, the number of wrinkles can be approximated using a "local λ" law which estimates the wrinkle number as a function of the effective stiffness of the floating film under tension.[67,68] The theory, which incorporates both the gravitational potential energy of the water and the radial tension in the film as stiffness terms that oppose the deformation of the film, predicts $N(r)$, the number of wrinkles as a function of radial distance from the contact line as

$$N(r) \approx r\left[\frac{\rho g + \left(\frac{\tau\gamma_{bath}a}{4r^3}\right)\left(\frac{\log(L/r)-1}{\log(L/r)}\right)^2}{B}\right]^{1/4} \tag{6}$$

$$\tau \approx \frac{\gamma}{\gamma_{bath}}\left(\frac{3}{10}\frac{\sin^2\theta}{x|\ln x|}\right)^{1/3} \tag{7}$$

where ρ is the density of water ($\rho = 1000$ kg/m^3), g is the gravitational acceleration ($g = 9.81$ m/s^2), γ_{bath} and γ are both identical in our case and equal to the surface tension of water since both the bath and the drop contain the same liquid, a is the radius of a water droplet, θ is the contact angle of the water droplet on the top surface of the film and $x = (\gamma/Y)$, where Y is the stretching modulus of the bilayer film. Physically, the confinement parameter, τ, is the ratio of the radial stresses at the edge of the drop, and at the outer edge of the film: $\tau \equiv \sigma_{rr}^{(o)}/\gamma$.

The theoretical prediction for N is a function of the radial distance from the edge of the drop, however, as shown in Figure 1, the number of wrinkles is uniform in the bulk of the wrinkle pattern. We apply these predictions to the measured wrinkle number at a radial distance halfway through the wrinkle pattern, i.e., at a radial distance given by $r = (a + L)/2$. The effective stretching modulus obtained from the wrinkle length, Y_{eff}, as a function of Y, and the effective bending modulus, B_{eff}, measured from the wrinkle number as a function of B were calculated for PS/PMMA, PMMA/PS, PS/Au, and Au/PS bilayer films using eq 2 for Y, eqs 5 and 7 with the Nsolve function in Mathematica for Y_{eff}, eq 4 for B, and eqs 6 and 7 for B_{eff}, respectively.

RESULT AND DISCUSSION

Figure 1 shows optical micrographs of the wrinkle patterns of PMMA (top)/PS (bottom), PS/PMMA, Au/PS, and PS/Au bilayer films, where it is seen that the number of wrinkles decreases, and the length of wrinkles increases as the film becomes stiffer. The dominant effect on both bending and in-

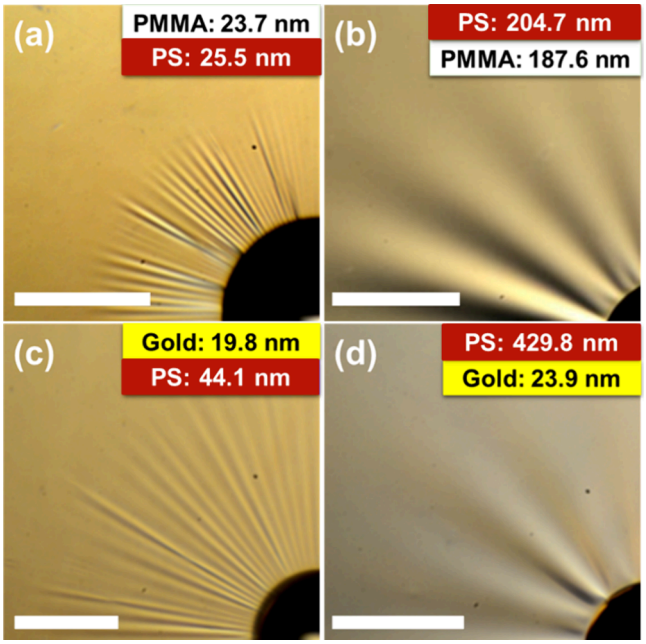

Figure 1. Wrinkle patterns on (a) a PMMA (top)/PS (bottom) thin bilayer film ($t_{total} = 49.2$ nm), (b) a PS/PMMA bilayer film ($t_{total} = 392.3$ nm), (c) an Au/PS thin bilayer film ($t_{total} = 63.9$ nm), and (d) a PS/Au bilayer film ($t_{total} = 453.7$ nm). Only one quadrant of the film is shown in each case. The drop is seen at the bottom right edge of each image, but the outer edges of the floating film are outside the image. Scale bars are all 1 mm.

https://doi.org/10.1021/acs.macromol.4c01540
Macromolecules 2024, 57, 10091−10097

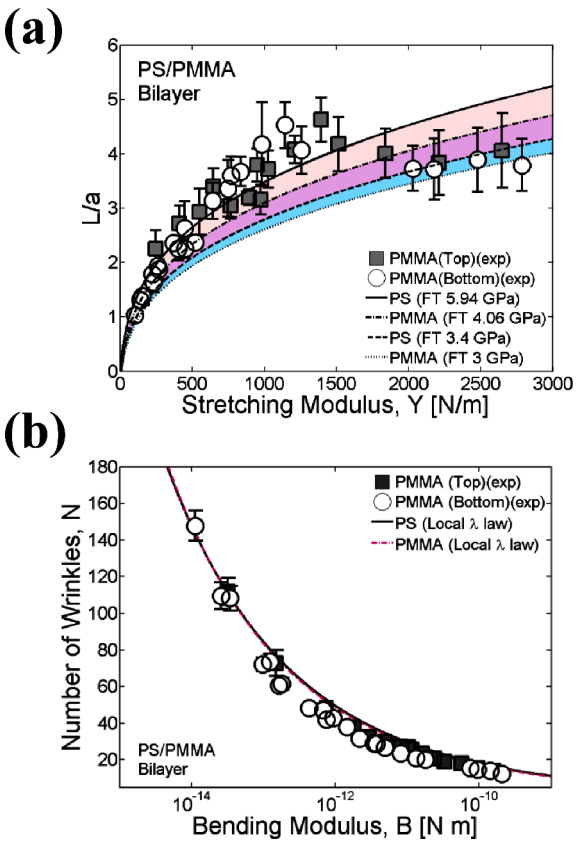

Figure 2. (a) Normalized length of wrinkles (L/a) vs stretching modulus (Y) of PS/PMMA and PMMA/PS bilayer films. Lines are calculated from eqs 1, 5, 7 using $E_{PS,exp}$ = 5.9 GPa and $\theta_{PS,}$ = 88° for a solid line, $E_{PMMA,exp}$ = 4.06 GPa and θ_{PMMA} = 68° for a dash-dotted line, $E_{PS,lit}$ = 3.4 GPa and θ_{PS} = 88° for a dashed line, and $E_{PMMA,lit}$ = 3.0 GPa and θ_{PMMA} = 68° for a dotted line, respectively. (b) Number of wrinkles (N) versus the bending modulus (B) of PS/PMMA and PMMA/PS bilayer systems. Black solid and red dash-dotted lines are obtained from eqs 1, 3, 6, 7 using $E_{PS,lit}$ = 3.4 GPa, $E_{PMMA,lit}$ = 3.0 GPa, and θ_{PS} = 88° for the black solid line and $E_{PS,lit}$ = 3.4 GPa, $E_{PMMA,lit}$ = 3.0 GPa and θ_{PMMA} = 68° for the red dash-dotted line, respectively.

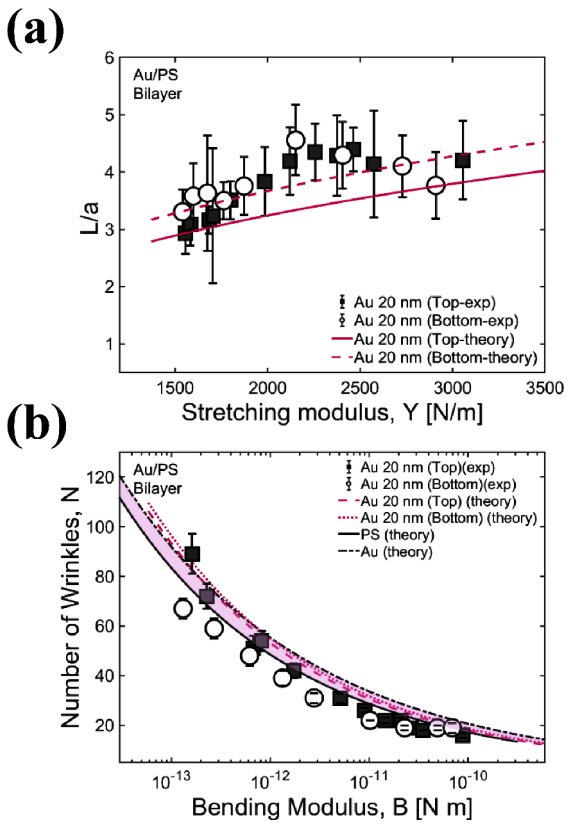

Figure 3. (a) Normalized length of wrinkles (L/a) versus stretching modulus (Y) of PS/Au and Au/PS bilayer films. Lines are calculated from eqs 2, 5, 7 using $E_{PS,lit}$ = 3.4 GPa, $E_{Au,lit}$ = 72 GPa, and θ_{Au} = 60° for a red solid line, $E_{PS,lit}$ = 3.4 GPa, $E_{Au,lit}$ = 72 GPa, and θ_{PS} = 88° for a red dash-dotted line, respectively. (b) Number of wrinkles (N) versus bending modulus (B) of PS/Au and Au/PS bilayer systems. Black solid and dash-dotted lines are obtained from eqs 1, 3, 6, 7 using $E_{PS,lit}$ = 3.4 GPa and θ_{PS} = 88°, and $E_{Au,lit}$ = 72 GPa and θ_{Au} = 60°, while red dashed and dotted lines are calculated using eqs 2, 4, 6, 7 with $E_{PS,lit}$ = 3.4 GPa, $E_{Au,lit}$ = 72 GPa, and θ_{PS} = 88°, and $E_{PS,lit}$ = 3.4 GPa, $E_{Au,lit}$ = 72 GPa and θ_{Au} = 60°, respectively.

plane rigidity comes from the thickness of the film. The bulk Young's moduli of the materials are important, and subtler effects appear via the contact angle.

In Figures 2a and 3a, we plot the normalized length (L/a) of the wrinkles in PS/PMMA and PS/Au bilayers, respectively. These are plotted against the expected effective stretching modulus Y, as calculated from the known elastic moduli and the chosen thicknesses of each of the two components in the bilayer using eq 2. Apart from the thicknesses of the film layers, the other experimental control variable is the drop radius, a. We confirmed that, as in previous work, the length L scales linearly with a, so the normalization in terms of L/a leaves no further dependence on a to account for.[23] Both in Figures 2a and 3a, within the error of the measurement, there is no noticeable difference between when one or the other of the two materials is on top. Thus, the dependence that enters through the contact angle does not make a strong difference. The lines in Figures 2a and 3a are theoretical curves from eqs 1, 5, 7 for Figures 2a and eqs 2, 5, 7 for Figure 3a, calculated with $E_{PS,experiment\ (exp)}$ = 5.94 GPa, $E_{PS,literature\ (lit)}$ = 3.4 GPa, θ_{PS} = 88°; $E_{PMMA,exp}$ = 4.06 GPa, $E_{PMMA,lit}$ = 3.0 GPa, θ_{PMMA} = 68°, $E_{Au,lit}$ = 72 GPa, and θ_{Au} = 60°.[67,69] Note that there are two curves for each bilayer system, corresponding to different experiments with different surfaces of the bilayer facing up, so that different values of the Young-Dupré angle, θ, need to be inserted in eqs 5 and 7. In Figure 2a, we show two values of Young's moduli for both PS and PMMA, one taken from literature on the bulk value, and another determined by us from measurements on single-layer films made by the same spin-coating protocols.[67] As can be seen, there is reasonable agreement between the prediction of eq 5 and the observations in Figures 2a and 3a. The largest disagreements are in Figure 2a at large values of Y, where the normalized wrinkle length (L/a) increases initially with thickness as expected but saturates for thicker films. We suggest that the saturation arises from a finite size effect, where the length of the wrinkle approaches the size of the bilayer film, whereas our expressions assume a film size that is much larger than the size of the wrinkle pattern.

In Figures 2b and 3b, we plot the measured wrinkled number $N(r)$, evaluated at the middle of the wrinkle pattern, against the expected value of the effective bending modulus B for the bilayer calculated by using eq 4. Once again, the smooth curves in each of the figures correspond to predictions from eqs 1, 3, 6, 7 for Figure 2b and eqs 1−4, 6, 7 for Figure 3b. The predictions for the measured wrinkle number N match the measurements reasonably well over a very large range of B (4 orders of magnitude for PS/PMMA and PMMA/PS bilayer films and

https://doi.org/10.1021/acs.macromol.4c01540
Macromolecules 2024, 57, 10091−10097

three orders of magnitude for the PS/Au and Au/PS films). There are small but systematic differences between the PS/Au and Au/PS bilayers, which we note were made by entirely different protocols.

As an example, Figure 4a and 4b show the comparison in a different way for the polymer-gold system. Here, we compare the experimentally measured values of the effective stretching moduli (Y_{eff}) and bending moduli (B_{eff}) (i.e., by using experimentally measured L and N, and numerically inverting eqs 5 and 7 for Y_{eff} and eqs 6 and 7 for B_{eff}) to the ones calculated from eqs 2 and 4 based on the known Young's moduli of PS and Au and film thicknesses. The experimental Y_{eff} and B_{eff} are comparable to the calculated values, Y_{eff} is higher than Y, yet B_{eff} is systematically lower for Au/PS bilayer films where $B \leq \sim 10^{-11}$ N m.[70,71] The calculation that results in eqs 5−7 which enables our ability to determine Y and B from L and $N(r)$, ignores some details that can have quantitative effects: first, the displacement boundary conditions at $r = a$ are quite complex in the experiment. Second, there is a boundary layer at the tip of the wrinkle where the curved portion meets the planar part of the film; this can contribute to the observed length of the wrinkle but is not included in eqs 5−7.[67]

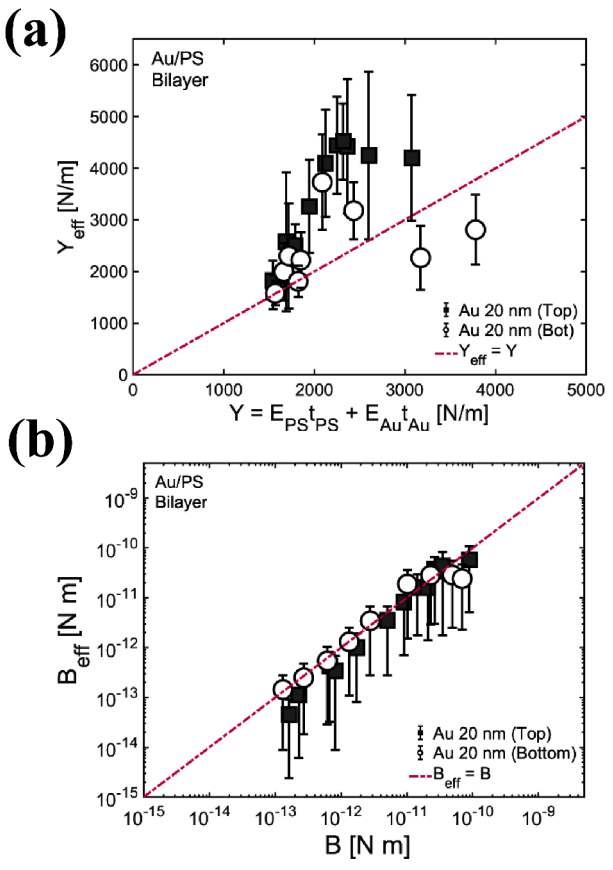

Figure 4. (a) Theoretical stretching modulus, Y, dependence of the effective stretching modulus, Y_{eff}, obtained from Au/PS and PS/Au bilayer films. Y was determined with eq 2 and Y_{eff} was quantified utilizing the experimental wrinkle lengths with eqs 5 and 7. (b) Theoretical bending modulus, B, dependence of the effective bending modulus, B_{eff}, measured with Au/PS and PS/Au bilayer films. The B and B_{eff} values were computed using eq 4 for B and eqs 6 and 7 for B_{eff}, respectively. $E_{PS,lit} = 3.4$ GPa, $E_{Au,lit} = 72$ GPa, $t_{Au} = 20$ nm and a t_{PS}, 29.6 nm $\leq t_{PS} \leq$ 475.2 nm, were used to calculate Y, Y_{eff}, B, and B_{eff}.

CONCLUSIONS

Our results show that the bending and stretching moduli of bilayer films, both polymer/polymer and polymer/Au, can be correctly determined by knowing the individual thicknesses and Young's moduli of the two layers. The moduli estimated from eqs 1 and 2 agree well with the moduli determined in our experimental data for the size and wavenumber of wrinkle patterns generated by capillary stresses. We have explicitly tested this agreement over a broad range of total film thickness for PMMA/PS and PS/PMMA (33.6 to 884.3 nm) and for PS/Au and Au/PS (49.6 to 495.2 nm) and ratios of the individual layer thicknesses. We account for the contrasts in wetting properties with different contact angles of $\theta_{PMMA} = 68°$, $\theta_{PS} = 88°$ and $\theta_{Au} = 60°$ and mechanical properties accompanied by different Young's moduli of $E_{PS} = 3.4$ GPa and $E_{Au} = 72$ GPa. Stretching and bending moduli for the PMMA/PS and PS/PMMA bilayer films responded like a single elastic object with no slippage at the interface between the two layers. This was also found to be true for PS/Au and Au/PS bilayer films; we do, however, see a small but systematic difference between these two types of film possibly because they were produced by entirely different protocols. From these results, we show that the combination of a classic bilayer model with formulas (Y and B) can be used to determine the mechanical properties of the bilayer films. In addition, these findings can be useful in cases where nonbulk effects are anticipated, widening perspectives beyond thin-film metrology.

AUTHOR INFORMATION

Corresponding Author

Thomas P. Russell − *Department of Polymer Science and Engineering, University of Massachusetts Amherst, Amherst, Massachusetts 01003, United States;* orcid.org/0000-0001-6384-5826; Email: russell@mail.pse.umass.edu

Authors

Jooyoung Chang − *Department of Polymer Science and Engineering, University of Massachusetts Amherst, Amherst, Massachusetts 01003, United States;* Present Address: Intel Corporation, Hillsboro, Oregon 97124, United States

Narayanan Menon − *Department of Physics, University of Massachusetts Amherst, Amherst, Massachusetts 01003, United States;* orcid.org/0000-0003-0901-8488

Complete contact information is available at: https://pubs.acs.org/10.1021/acs.macromol.4c01540

Notes

The authors declare no competing financial interest.

ACKNOWLEDGMENTS

This work was supported by the US Army Research Office under contract W911NF-24-2-0041, the W.M. Keck Foundation, and NSF grants 2226310 and 1905698. We thank Y. Kim, B. Davidovitch, D. Vella, D. Kumar, Y. Liu, H. Lee, D. Waldman, S. Chantarak, J. Choi, J. Patel, D.M. Yu, H. Kim, S. Srivastava, Z. Fink, S. Lee, I. Chang, E. Chang, S. Chang, M. Park, J. Chang, Y. Son, H. Lee, D. Lee, and J. Rusnock for fruitful discussions. This manuscript is adapted from Chapter 3 of Jooyoung Chang's Ph.D. thesis, titled "The Effect of Bulk Modulus, Surface Energy, and Thickness on Wrinkle Patterns and Young's Modulus of Bilayer Films". 10.7275/jevc-yj26

https://doi.org/10.1021/acs.macromol.4c01540
Macromolecules 2024, 57, 10091−10097

REFERENCES

(1) Brown, H. R.; Russell, T. P. Entanglements at Polymer Surfaces and Interfaces. *Macromoelcules* **1996**, *29*, 798−800.
(2) Lu, H.; Chen, W.; Russell, T. P. Relaxation of Thin Films of Polystyrene Floating on Ionic Liquid Surface. *Macromolecules* **2009**, *42*, 9111−9117.
(3) Plazek, D. J. Temperature Dependence of the Viscoelastic Behavior of Polystyrene. *J. Phys. Chem.* **1965**, *69*, 3480−3487.
(4) Alcoutlabi, M.; McKenna, G. B. Effects of Confinement on Material Behaviour at the Nanometre Size Scale. *J. Phys.: Condens. Matter* **2005**, *17*, R461−R524.
(5) Yoon, H.; Mckenna, G. B. Substrate Effects on Glass Transition and Free Surface Viscoelasticity of Ultrathin Polystyrene Films. *Macromolecules* **2014**, *47*, 8808−8818.
(6) Li, X.; McKenna, G. B. Ultrathin Polymer Films: Rubbery Stiffening, Fragility, and T g Reduction. *Macromolecules* **2015**, *48*, 6329−6336.
(7) Majeste, J. C.; Montfort, J. P.; Allal, A.; Marin, G. Viscoelasticity of Low Molecular Weight Polymers and the Transition to the Entangled Regime. *Rheol. Acta* **1998**, *37*, 486−499.
(8) King, H.; Schroll, R. D.; Davidovitch, B.; Menon, N. Elastic Sheet on a Liquid Drop Reveals Wrinkling and Crumpling as Distinct Symmetry-Breaking Instabilities. *Proc. Natl. Acad. Sci. U. S. A.* **2012**, *109*, 9716−9720.
(9) King, J. S.; Boyer, W.; Wignall, G. D.; Ullman, R. Radii of Gyration and Screening Lengths of Polystyrene in Toluene as a Function of Concentration. *Macromolecules* **1985**, *18*, 709−718.
(10) Cerda, E.; Mahadevan, L. Geometry and Physics of Wrinkling. *Phys. Rev. Lett.* **2003**, *90* (7), No. 074302.
(11) Xia, W.; Keten, S. Interfacial Stiffening of Polymer Thin Films under Nanoconfinement. *Extreme Mech Lett.* **2015**, *4*, 89−95.
(12) Vella, D.; Adda-Bedia, M.; Cerda, E. Capillary Wrinkling of Elastic Membranes. *Soft Matter* **2010**, *6*, 5778.
(13) Paeng, K.; Ediger, M. D. Molecular Motion in Free-Standing Thin Films of Poly(Methyl Methacrylate), Poly(4-Tert-Butylstyrene), Poly(α-Methylstyrene), and Poly(2- Vinylpyridine). *Macromolecules* **2011**, *44*, 7034−7042.
(14) Lee, H.; Paeng, K.; Swallen, F.; Stephen, M. D. E. Direct Measurement of Molecular Mobility in Actively Deformed Polymer Glasses. *Science* **2009**, *323*, 231−234.
(15) Paeng, K.; Swallen, S. F.; Ediger, M. D. Direct Measurement of Molecular Motion in Freestanding Polystyrene Thin Films. *J. Am. Chem. Soc.* **2011**, *133*, 8444−8447.
(16) Rittigstein, P.; Priestley, R. D.; Broadbelt, L. J.; Torkelson, J. M. Model Polymer Nanocomposites Provide an Understanding of Confinement Effects in Real Nanocomposites. *Nat. Mater.* **2007**, *6*, 278−282.
(17) Priestley, R. D.; Ellison, C. J.; Broadbelt, L. J.; Torkelson, J. M. Structural Relaxation of Polymer Glasses at Surfaces, Interfaces, and in Between. *Science* **1979**, *2005* (309), 456−459.
(18) Roth, C. B.; McNerny, K. L.; Jager, W. F.; Torkelson, J. M. Eliminating the Enhanced Mobility at the Free Surface of Polystyrene: Fluorescence Studies of the Glass Transition Temperature in Thin Bilayer Films of Immiscible Polymers. *Macromolecules* **2007**, *40*, 2568−2574.
(19) Ellison, C. J.; Torkelson, J. M. The Distribution of Glass-Transition Temperatures in Nanoscopically Confined Glass Formers. *Nat. Mater.* **2003**, *2*, 695−700.
(20) Torres, J. M.; Stafford, C. M.; Vogt, B. D. Elastic Modulus of Amorphous Polymer Thin Films: Relationship to the Glass Transition Temperature. *ACS Nano* **2009**, *3*, 2677−2685.
(21) Torres, J. M.; Stafford, C. M.; Vogt, B. D. Impact of Molecular Mass on the Elastic Modulus of Thin Polystyrene Films. *Polymer* **2010**, *51*, 4211−4217.
(22) Bowden, N.; Brittain, S.; Evans, A. G.; Hutchinson, J. W.; Whitesides, G. M. Spontaneous Formation of Ordered Structures in Thin Films of Metals Supported on an Elastomeric Polymer. *Nature* **1998**, *393*, 146−149.
(23) Huang, J.; Juszkiewicz, M.; De Jeu, W. H.; Cerda, E.; Emrick, T.; Menon, N.; Russell, T. P. Capillary Wrinkling of Floating Thin Polymer Films. *Science* **1979**, *2007* (317), 650−653.
(24) Toga, K. B.; Huang, J.; Cunningham, K.; Russell, T. P.; Menon, N. A Drop on a Floating Sheet: Boundary Conditions, Topography and Formation of Wrinkles. *Soft Matter* **2013**, *9*, 8289−8296.
(25) Kerle, T.; Lin, Z.; Kim, H.; Russell, T. P. Mobility of Polymers at the Air/Polymer Interface. *Macromolecules* **2001**, *34*, 3484−3492.
(26) Jones, R.; Kumar, S.; Ho, D.; Briber, R.; Russell, T. Chain Conformation in Ultrathin Polymer Films. *Nature* **1999**, *400*, 146−149.
(27) Stafford, C. M.; Harrison, C.; Beers, K. L.; Karim, A.; Amis, E. J.; VanLandingham, M. R.; Kim, H.-C.; Volksen, W.; Miller, R. D.; Simonyi, E. E. A Buckling-Based Metrology for Measuring the Elastic Moduli of Polymeric Thin Films. *Nat. Mater.* **2004**, *3*, 545−550.
(28) Stafford, C. M.; Vogt, B. D.; Harrison, C.; Julthongpiput, D.; Huang, R. Elastic Moduli of Ultrathin Amorphous Polymer Films. *Macromolecules* **2006**, *39*, 5095−5099.
(29) O'Connell, P. A.; McKenna, G. B. Rheological Measurements of the Thermoviscoelastic Response of Ultrathin Polymer Films. *Science* **1979**, *2005* (307), 1760−1763.
(30) O'Connell, P. A.; Mckenna, G. B. A Novel Nano-Bubble Inflation Method for Determining the Viscoelastic Properties of Ultrathin Polymer Films. *Scanning* **2008**, *30*, 184−196.
(31) O'Connell, P. A.; McKenna, G. B. Dramatic Stiffening of Ultrathin Polymer Films in the Rubbery Regime. *Eur. Phys. J. E* **2006**, *20*, 143−150.
(32) Zhao, J. H.; Kiene, M.; Hu, C.; Ho, P. S. Thermal Stress and Glass Transition of Ultrathin Polystyrene Films. *Appl. Phys. Lett.* **2000**, *77*, 2843−2845.
(33) Liu, Y.; Chen, Y. C.; Hutchens, S.; Lawrence, J.; Emrick, T.; Crosby, A. J. Directly Measuring the Complete Stress-Strain Response of Ultrathin Polymer Films. *Macromolecules* **2015**, *48*, 6534−6540.
(34) Kim, J.-H.; Nizami, A.; Hwangbo, Y.; Jang, B.; Lee, H.-J.; Woo, C.-S.; Hyun, S.; Kim, T.-S. Tensile Testing of Ultra-Thin Films on Water Surface. *Nat. Commun.* **2013**, *4*, 1−6.
(35) Forrest, J. A.; Veress, K. D.; Dutcher, J. R. Brillouin Light Scattering Studies of the Mechanical Properties of Thin Freely Standing Polystyrene Films. *Phys. Rev. E* **1998**, *58*, 6109−6114.
(36) DeMaggio, G.; Frieze, W.; Gidley, D.; Zhu, M.; Hristov, H.; Yee, A. F. Interface and Surface Effects on the Glass Transition in Thin Polystyrene Films. *Phys. Rev. Lett.* **1997**, *78*, 1524−1527.
(37) Mansfield, K. F.; Theodorou, D. N. Atomistic Simulation of a Glassy Polymer Surface. *Macromolecules* **1990**, *23*, 4430−4445.
(38) Maillard, D.; Kumar, S. K.; Fragneaud, B.; Kysar, J. W.; Rungta, A.; Benicewicz, B. C.; Deng, H.; Brinson, L. C.; Douglas, J. F. Mechanical Properties of Thin Glassy Polymer Films Filled with Spherical Polymer-Grafted Nanoparticles. *Nano Lett.* **2012**, *12*, 3909−3914.
(39) Wallace, W. E.; Van Zanten, J. H.; Wu, W. L. Influence of an Impenetrable Interface on a Polymer Glass-Transition Temperature. *Phys. Rev. E* **1995**, *52*, R3329−R3332.
(40) Tsui, O. K. C.; Wang, X. P.; Ho, J. Y. L.; Ng, T. K.; Xiao, X. Studying Surface Glass-to-Rubber Transition Using Atomic Force Microscopic Adhesion Measurements. *Macromolecules* **2000**, *33*, 4198−4204.
(41) Kawana, S.; Jones, R. A. L. Character of the Glass Transition in Thin Supported Polymer Films. *Phys. Rev. E* **2001**, *63*, No. 021501.
(42) Tran, T. A.; Saïd, S.; Grohens, Y. Nanoscale Characteristic Length at the Glass Transition in Confined Syndiotactic Poly(Methyl Methacrylate). *Macromolecules* **2005**, *38*, 3867−3871.
(43) Kremer, F.; Tress, M.; Mapesa, E. U. Glassy Dynamics and Glass Transition in Nanometric Layers and Films: A Silver Lining on the Horizon. *J. Non Cryst. Solids* **2015**, *407*, 277−283.
(44) Forrest, J. A.; Dalnoki-Veress, K. The Glass Transition in Thin Polymer Films. *Adv. Colloid Interface Sci.* **2001**, *94*, 167−196.
(45) Wang, J.; McKenna, G. B. Viscoelastic Properties of Ultrathin Polycarbonate Films by Liquid Dewetting. *J. Polym. Sci. B Polym. Phys.* **2015**, *53*, 1559−1566.

https://doi.org/10.1021/acs.macromol.4c01540
Macromolecules 2024, 57, 10091−10097

(46) Jones, R. L.; Kumar, S. K.; Ho, D. L.; Briber, R. M.; Russell, T. P. Chain Conformation in Ultrathin Polymer Films Using Small-Angle Neutron Scattering. *Macromolecules* **2001**, *34*, 559−567.
(47) Tweedie, C. A.; Constantinides, G.; Lehman, K. E.; Brill, D. J.; Blackman, G. S.; Van Vliet, K. J. Enhanced Stiffness of Amorphous Polymer Surfaces under Confinement of Localized Contact Loads. *Adv. Mater.* **2007**, *19*, 2540−2546.
(48) Lee, J. H.; Chung, J. Y.; Stafford, C. M. Effect of Confinement on Stiffness and Fracture of Thin Amorphous Polymer Films. *ACS Macro Lett.* **2012**, *1*, 122−126.
(49) Stafford, C. M.; Harrison, C.; Beers, K. L.; Karim, A.; Amis, E. J.; Vanlandingham, M. R.; Kim, H. C.; Volksen, W.; Miller, R. D.; Simonyi, E. E. A Buckling-Based Metrology for Measuring the Elastic Moduli of Polymeric Thin Films. *Nat. Mater.* **2004**, *3*, 545−550.
(50) Page, K. A.; Kusoglu, A.; Stafford, C. M.; Kim, S.; Kline, R. J.; Weber, A. Z. Confinement-Driven Increase in Ionomer Thin-Film Modulus. *Nano Lett.* **2014**, *14*, 2299−2304.
(51) Torkelson, J. M.; Lipsky, S.; Tirrell, M. Polystyrene Fluorescence: Effects of Molecular Weight in Various Solvents. *Macromolecules* **1981**, *14*, 1601−1603.
(52) Du, B.; Tsui, O. K. C.; Zhang, Q.; He, T. Study of Elastic Modulus and Yield Strength of Polymer Thin Films Using Atomic Force Microscopy. *Langmuir* **2001**, *17*, 3286−3291.
(53) Maillard, D.; Kumar, S. K.; Rungta, A.; Benicewicz, B. C.; Prud'Homme, R. E. Polymer-Grafted-Nanoparticle Surfactants. *Nano Lett.* **2011**, *11*, 4569−4573.
(54) Bodiguel, H.; Fretigny, C. Reduced Viscosity in Thin Polymer Films. *Phys. Rev. Lett.* **2006**, *97*, 1−4.
(55) Bodiguel, H.; Fretigny, C. Viscoelastic Dewetting of a Polymer Film on a Liquid Substrate. *Eur. Phys. J. E* **2006**, *19*, 185−193.
(56) Bodiguel, H.; Fretigny, C. Viscoelastic Properties of Ultrathin Polystyrene Films. *Macromolecules* **2007**, *40*, 7291−7298.
(57) Wang, J.; McKenna, G. B. Viscoelastic and Glass Transition Properties of Ultrathin Polystyrene Films by Dewetting from Liquid Glycerol. *Macromolecules* **2013**, *46*, 2485−2495.
(58) Madhusudanan, M.; Chowdhury, M. Advancements in Novel Mechano-Rheological Probes for Studying Glassy Dynamics in Nanoconfined Thin Polymer Films. *ACS Polymers Au* **2024**, *4*, 342.
(59) Schroll, R. D.; Adda-Bedia, M.; Cerda, E.; Huang, J.; Menon, N.; Russell, T. P.; Toga, K. B.; Vella, D.; Davidovitch, B. Capillary Deformations of Bendable Films. *Phys. Rev. Lett.* **2013**, *111*, No. 014301.
(60) Ennis, D.; Heike, B.; Ade, H. Direct Spincasting of Polystyrene Thin Films onto Poly(Methyl Methacrylate). *J. Polym. Sci. B Polym. Phys.* **2006**, *44* (22), 3234−3244.
(61) Yoon, H.; McKenna, G. B. Substrate Effects on Glass Transition and Free Surface Viscoelasticity of Ultrathin Polystyrene Films. *Macromolecules* **2014**, *47*, 8808−8818.
(62) Whitney, J. M. *Structural Analysis of Laminated Anisotropic Plates*; Technomic: Lancaster, 1987.
(63) Avilés, F.; Oliva, A. I.; May-Pat, A. Determination of Elastic Modulus in a Bimaterial through a One-Dimensional Laminated Model. *J. Mater. Eng. Perform* **2008**, *17* (4), 482−488.
(64) Allen, H. *Analysis and Design of Structural Sandwich Panels*; Pergamon Press: New York, 1969.
(65) Kumar, D.; Russell, T. P.; Davidovitch, B.; Menon, N. Stresses in Thin Sheets at Fluid Interfaces. *Nat. Mater.* **2020**, *19* (7), 690−693.
(66) Davidovitch, B.; Schroll, R. D.; Vella, D.; Adda-Bedia, M.; Cerda, E. A. Prototypical Model for Tensional Wrinkling in Thin Sheets. *Proc. Natl. Acad. Sci. U. S. A.* **2011**, *108*, 18227−18232.
(67) Chang, J.; Toga, K. B.; Paulsen, J. D.; Menon, N.; Russell, T. P. Thickness Dependence of the Young's Modulus of Polymer Thin Films Macromolecules. *Macromolecules* **2018**, *51*, 6764−6770.
(68) Paulsen, J. D.; Hohlfeld, E.; King, H.; Huang, J.; Qiu, Z.; Russell, T. P.; Menon, N.; Vella, D.; Davidovitch, B. Curvature-Induced Stiffness and the Spatial Variation of Wavelength in Wrinkled Sheets. *Proc. Natl. Acad. Sci. U. S. A.* **2016**, *113*, 1144−1149.
(69) Wang, L.; Liang, C.; Prorok, B. C. A Comparison of Testing Methods in Assessing the Elastic Properties of Sputter-Deposited Gold Films. *Thin Solid Films* **2007**, *515*, 7911−7918.
(70) Landau, L.; Lifshitz, E. *Theory of Elasticity*; 1986.
(71) Timoshenko, S.; Goodier, J. N. *Theory of Elasticity*, 3rd ed.; McGraw-Hil: New York, 1969.

https://doi.org/10.1021/acs.macromol.4c01540
Macromolecules 2024, 57, 10091−10097